The Role of Large Scale Mixing and Radiation in the Scaling of NOx Emissions From Unconfined Flames

Greg J.R. Newbold, Graham J. Nathan and David S. Nobes
Department of Mechanical Engineering
Adelaide University
Adelaide 5005, Australia

Stephen R. Turns
Department of Mechanical and Nuclear Engineering
The Pennsylvania State University
University Park, PA 16802, USA

ABSTRACT

Measurements of global emissions, flame radiation and flame dimensions are presented for unconfined turbulent-jet and precessing-jet diffusion flames. Precessing jet flames are characterised by increases in global flame radiation and global flame residence time for methane and propane fuels, however a strong dependency of the NOx emission indices on the fuel type exists. The fuel type dependence is considered to be because soot radiation is more effective than gas-radiation at reducing global flame temperatures relative to adiabatic flame temperatures and reducing the NO production rate.

Keywords : diffusion flames, NOx, radiation, turbulent-jet, precessing-jet.

NOMENCLATURE

d_f	Fuel tube diameter
d_f^*	Fuel tube momentum diameter
f_s	Mass fraction of fuel in a stoichiometric mixture
Fr	Froude number
L_f	Fuel tube length
L_{Flame}	Flame length
Re_d	Reynolds number
τ_G	Global residence time ($\propto L_{Flame}\, W_{Flame}^2$ / $u_f\, d_f^2$)
τ_R	Residence time (= L_{Flame}^3 / $u_f\, d_f^2$)
u_f	Fuel jet velocity
W_{Flame}	Flame width
χ_r	Radiant fraction

INTRODUCTION

NO_x emissions from combustion sources are a significant pollution source. Models have been developed to explain global NO_x emis-

sions trends for turbulent-jet diffusion flames [1-9]. These models consider the dominant physical mechanisms that influence NO production via the thermal and prompt mechanisms, so that scaling of NO_x emissions from turbulent-jet flames can be considered with respect to global flame parameters.

A flamelet model has been developed [1] that correlates the NO_x emissions of hydrogen flames with the residence time, τ_R [2,3]. These flames do not include prompt NO_x chemistry, effects of soot and radiation from these flames is purely gas chromatic, with radiant fractions of about 8%. However, hydrogen flames with coaxial air are not fully correlated by the model, and this has been attributed to the effect of radiation [11].

The effect of flame radiation has been included in a time-temperature model [7]. The NO_x emissions from hydrogen and hydrocarbon flames are correlated with the global flame temperature by a thermal NO_x model, derived from the adiabatic flame temperature corrected for the measured radiant heat losses. However, a strained laminar diffusion flamelet model that does not consider radiation has also been used to correlate the emission index with Froude number, Fr [4,5].

All the global emission models provide reasonable agreement in scaling for propane turbulent-jet flames [10]. The propane flames investigated included the variable effects of buoyancy, prompt NO_x chemistry and soot. It has been proposed that the quantitatively similar effect of buoyancy (through Fr) and flame radiation (through the global flame temperature) explain why the models yield similar results [8].

NO_x emission models have been developed for turbulent-jet flames, and have been evaluated for propane flames with widely different fuel jet mixing [10]. NO_x emissions from a bluff-body, a swirl and a precessing jet burners are scaled by the time-temperature model [7], though a departure of the data from predictions based on the theoretical thermal NO production rate, d[NO] / dt (for $N_2 + O \Leftrightarrow N + NO$ and $N + O_2 \Leftrightarrow NO + O$), is found.

Experimental measurements are used here to consider the NO_x models in relation to turbulent-jet and precessing-jet flames and to explore the effect of significant departures from mixing similarity on the global flame characteristics, including radiation and NO_x formation.

EXPERIMENTAL METHODS

Measurements were conducted in a $1.2 \times 1.2 \times 3.5$m mesh enclosure [10]. Flame photographs, global emissions (NO, NO_2, CO, CO_2 and unburned hydrocarbons) and single-point total flame radiation were measured for each flame using methods described elsewhere [10]. The NO_x data were converted from concentration levels to an emission index, $EINO_x$ (g [NO_x] / kg [Fuel]), with repeatability of $\pm$ 6%. Radiation measurements are converted to radiant fractions, χ_r, and are the fraction of the total energy of combustion radiated to the surroundings.

The turbulent-jet burner (Fig 1a) is a fuel tube, d_f = 5.0mm, with a long development length, L_f / d_f = 100, to ensure fully developed pipe flow at the exit. The precessing-jet burner uses an aerodynamic instability to cause a jet to precess about the nozzle axis [12]. A jet flows into a short axi-symmetric chamber section through an abrupt expansion (Fig 1b). The jet flow reattaches asymmetrically within the chamber and the associated asymmetric pressure field causes an azimuthal rotation

(precession) of the entire flow. An optimal geometric configuration for stable precession includes the addition an exit lip and a centre-body, with $Re_d \geq 20{,}000$ necessary at the jet throat [13]. The precessing-jet flow emerging from the nozzle is inclined to the nozzle axis at about 45° and precesses about it in a quasi-periodic manner.

Commercial propane and methane were used for the experiments. The fuels were metered through calibrated rotameters from a bottled supply. Turbulent-jet diffusion flames have been investigated for propane for the range $6 \leq u_f \leq 60$m/s ($7{,}000 \leq Re_d \leq 70{,}000$) and for methane for the range $35 \leq u_f \leq 70$m/s ($10{,}000 \leq Re_d \leq 20{,}000$), corresponding to the upper stability limit (blow-off). Precessing-jet flames have been investigated for the range of flow rates where stable precession is found to occur, $Re_d \geq 20{,}000$.

RESULTS

Turbulent-Jet Flames and NO_x Scaling

Images of the flames from the turbulent-jet and the precessing-jet burners are shown in Fig 1(c-f), for each fuel type and at Re_d = 20,000. Visible differences between the flames are apparent for these identical source conditions. Precession of a jet flow results in wide initial flame spread and an increase in flame width, which is related to the dominant role of large scale buoyant structures [14]. A trend of increased soot luminosity is also observed, in agreement with results for mechanical precessing-jet flames, with high precession frequency (Strouhal number) [15].

Flame length measurements are shown in Fig 2(a). It is observed that L_{Flame} increases monotonically with u_f for the turbulent-jet flames. Turbulent-jet flames are pure momentum dominated at $L_{Flame} f_s / d_f^* = 23$ [16]. The present methane and propane turbulent-jet flames are nearly momentum-dominated at the highest velocities, with $(L_{Flame} f_s / d_f^*)_{max} = 14$. The maximum fuel velocity for the turbulent jet is limited to $u_f = 70$ m/s by blow-off when firing methane. The maximum velocity when firing propane is limited by the experimental apparatus. Methane precessing-jet flames are stable at higher fuel jet velocities than are turbulent-jet flames, allowing $(u_f)_{max} = 140$ m/s. Calculations demonstrate that a stable flame is possible with choked flow at the nozzle chamber inlet for nozzles of all scales and fuel types. Interestingly, jet precession results in a reduction in L_{Flame} only for the propane flame case, and for methane the L_{Flame} are comparable for both nozzles. The propane turbulent-jet flame width-to-length ratios, W_{Flame} / L_{Flame}, shown in Fig 2(b), are consistent with a published value of $W_{Flame} / L_{Flame} = 0.17$ [7], though the methane flames spread slightly less, with $W_{Flame} / L_{Flame} = 0.14$. However, the precessing-jet flames have width-to-length ratios about twice that of turbulent-jet flames, with $W_{Flame} / L_{Flame} \approx 0.32$ for both fuels. Similar results of $W_{Flame} / L_{Flame} = 0.31$ and $W_{Flame} / L_{Flame} \approx 0.33$ are found for a precessing-jet flame from a burner with d_f = 2.3mm [14], and mechanical precessing-jet flames [15], respectively.

It is observed that the propane turbulent-jet flames are yellow and luminous for the u_f range considered, and a significant reduction in χ_r with fuel jet velocity, or strain rate ($= u_f / d_f$), is found (Fig 3a). In contrast, methane turbulent-jet flames, which are predominantly blue with minimal luminous soot, have low χ_r that are almost independent of u_f and can be deduced to have high global flame temperatures. Importantly, in parallel with changes in

flame luminosity, precession of a jet acts to increase χ_r for both fuels. For the propane case the peak value of χ_r equals that found for buoyancy dominated turbulent-jet flames, consistent with the buoyant nature of these flames. Precessing-jet flames demonstrate slight increases in χ_r with increasing u_f.

Measurements of NO_x emissions are shown in Fig 3(b). The propane turbulent-jet data show an $EINO_x$ dependence on u_f and the scaling of this data has been previously discussed [10]. $EINO_x$ values for the methane turbulent-jet flames are weakly dependent on u_f, showing a decrease in $EINO_x$ with increasing u_f, in agreement with results for the d_f = 0.386mm and d_f = 0.412mm turbulent-jet burners [7]. The propane precessing-jet flame is shown to reduce NO_x emissions compared with turbulent-jet flames, in contrast to methane precessing-jet flames. Mechanical jet precession can also increase χ_r and reduce $EINO_x$ by maximum values of 15% and 25%, respectively [15].

DISCUSSION

The role of radiation and large scale jet mixing in NO formation with respect to the present flames are further discussed. The χ_r of momentum dominated non-sooting turbulent-jet flames are expected to increase with τ_G, assuming optically thin flames [7]. The highly luminous propane turbulent-jet flames show that χ_r tends to scale with τ_G (Fig 4) in agreement with this model. However, momentum-dominated turbulent-jet flames are generally characterised by insignificant soot luminosity and lower χ_r than are buoyancy dominated flames and so are better described by this model, so that the dominant effect observed is related to the sooting tendency of propane. Since τ_G is inversely related to strain rate, the present results are also consistent with the observed decrease in soot volume fraction with increasing strain rate for laminar flames [17]. The methane turbulent-jet flames span a relatively small range of τ_G, and nearly constant χ_r is found, so that the present data are not readily scaled with the model. Comparison of the turbulent-jet and precessing-jet data further demonstrates a relationship between χ_r and τ_G. Importantly, the increase in χ_r for this class of flames is associated with an increase in τ_G.

The present turbulent-jet measurements can be scaled with respect to the flamelet model [1] and the strained laminar diffusion flamelet model [4,5], however the models do not explain differences between the methane (not shown) and propane (shown in [10]) data. Comparison of the present data with the time-temperature model [7] is presented in Fig 5, where a significant dependence of the NO production rate on fuel type and at similar global flame temperatures is found. The solid line represents the theoretical thermal NO production rate. For luminous propane turbulent-jet flames, which can be considered to be soot radiation dominated, an opposite trend is found for χ_r and $EINO_x$ with respect to uf (Fig 3). The measurements are consistent with the effect of changes to the global peak flame temperature by flame radiation on thermal NO_x production [6], despite a contribution of prompt NO_x to the emission. For the gas-radiation dominated methane flames $EINO_x$ is only weakly dependent on u_f while χ_r is relatively low and almost constant. At the high flame temperatures that can be inferred NO_x production is then insensitive to changes in χ_r. and is significantly dependent on τ_G, which is consistent with findings for gas radia-

tion dominated hydrogen flames [2,3,11]. The effect of soot radiation tends to dominate in the more luminous propane flames, but the dependence on τ_G tends to dominate in methane flames.

For the precessing-jet flames the same two competing influences are present. They provide an increase in both χ_r and τ_G in comparison with the turbulent-jet flames. Evidently the influence of increased soot radiation and lowering the flame temperature, dominates for the propane flames since the $EINO_x$ reduces. In contrast, for the methane flames, although χ_r increases for the precessing-jet flames relative to the turbulent-jet flames, the increase is not as great as for the propane flame. It is evident that the effect of increasing χ_r (and reducing $EINO_x$) is outweighed by the effect of increasing τ_G (and increasing $EINO_x$), which is not readily explained by the time-temperature model.

A comparison of NO_x emissions from a turbulent-jet burner with those from a precessing-jet burner was performed firing natural gas (commercial grade CH_4) in an 20MW operating cement kiln [18]. Although ambiguous boundary conditions are inherent in full-scale trials, the precessing-jet nozzle provided about a 40% reduction in NO_x emissions relative to the turbulent-jet flame, in contrast to the present results. A significant increase in χ_r can be deduced from the 4% increase in specific fuel efficiency and the 10% increase in kiln output. The present experiments were conducted in ambient air, whilst a cement kiln is confined so that the effects of buoyancy are minimal, and the air was preheated to around 900℃, so that thermal NO_x dominates and flame luminosity is increased. The differing role of soot and gas radiation on the global flame temperatures could explain why the dependence of $EINO_x$ on χ_r dominates over the dependence on τ_G.

CONCLUSIONS

Global emissions, flame radiation and flame dimensions of turbulent-jet flames are presented, which are consistent with published data. Precessing jet flames are characterised by increases in flame radiation and flame residence time for methane and propane, however a strong dependency of the NO_x emission indices on the fuel type exists. In propane flames radiation reduces the peak global flame temperature and thermal NO_x production compared with the turbulent jet flames. In methane flames residence time changes are more significant, suggesting that gas-radiation is less effective at reducing flame temperatures than soot-radiation.

Acknowledgement

This research was supported by the Australian DIST International Travel Programs. The contribution of Ramu Bandaru and Larry Schaff at PSU is gratefully acknowledged.

REFERENCES

1. Peters, N., and Donnerhack, S., *Proc. Comb. Inst.*, Vol. 18, pp. 33-42 (1981).
2. Chen, R. H., and Driscoll, J. F., *Proc. Comb. Inst.*, Vol. 23, pp. 281-288 (1990).
3. Driscoll, J. F., Chen, R. H., and Yoon, Y., *Combust. Flame*, Vol. 88, pp. 37-49 (1992).
4. Rokke, N. A., Hustad, J. E., Sonju, O. K., and Williams, F. A., *Proc. Comb. Inst.*, Vol. 24, pp. 385-393 (1992).
5. Rokke, N. A., Hustad, J. E., and Sonju, O. K., *Combust. Flame*, Vol. 97, pp. 88-106 (1994).

6. Turns, S. R., and Lovett, J. A., *Combust. Sci. Tech.*, Vol. 66, pp. 233-249 (1986).
7. Turns, S. R., and Myhr, F. H., *Combust. Flame*, Vol. 87:319-335 (1991).
8. Turns, S. R., *Prog. Energy. Combust. Sci.*, Vol. 21, pp. 361-385 (1995).
9. Broadwell, J. E., and Lutz, A. E., *Combust. Flame*, Vol. 114, pp. 319-335 (1998).
10. Newbold, G. J.R., Nathan, G. J., Nobes, D. S., and Turns, S. R., *Proc. Comb. Inst.*, Vol. 28 (2000).
11. Kim, S-H., Yoon, Y., and Jeung, I-S., *Proc. Comb. Inst.* Vol. 28 (2000)
12. Nathan, G. J., Hill, S. J, and Luxton, R. E., *J. Fluid Mech.*, Vol. 370, pp.347-380 (1998).
13. Hill, S. J., Nathan, G. J., and Luxton, R. E., *11th Australasian Fluid Mechanics Conference*, pp. 1113-1116 (1992).
14. Newbold, G. J.R., Nathan, G. J., and Luxton, R. E., *Combust. Sci. Tech.*, Vol. 126(1-6) pp. 71-95 (1997).
15. Nathan, G. J., Turns, S. R., and Bandaru, R. V., *Combust. Sci. Tech.*, Vol. 112, pp. 211-230 (1996).
16. Turns, S. R., *An Introduction to Combustion*, McGraw-Hill (1996).
17. Kent, J. H., and Bastin, S. J., *Comb. Flame* Vol. 56, pp. 29-42(1984).
18. Manias, C. G., and Nathan, G. J., *World Cement*, Vol. 24(3), pp. 4-11 (1993).

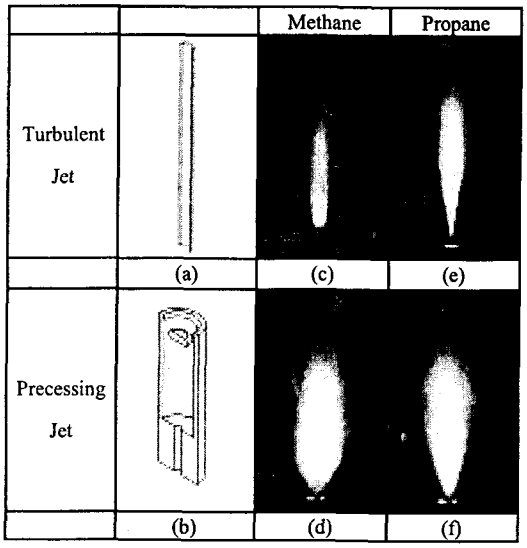

Figure 1. Long exposure (8 second) photographic images of turbulent-jet and precessing-jet flames of methane and propane at a jet Reynolds number Red = 20,000.

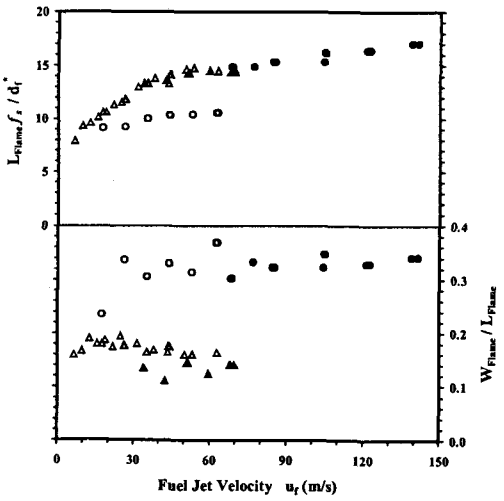

Figure 2. Flame length and width-to-length. ● Precessing-jet; ▲ Turbulent-jet (Open symbols: C_3H_8; closed: CH_4).

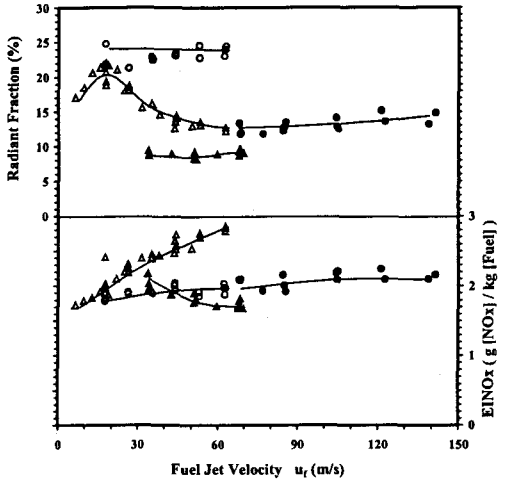

Figure 3. Radiant fractions and NOx emission indicies (Legend as for Fig. 2).

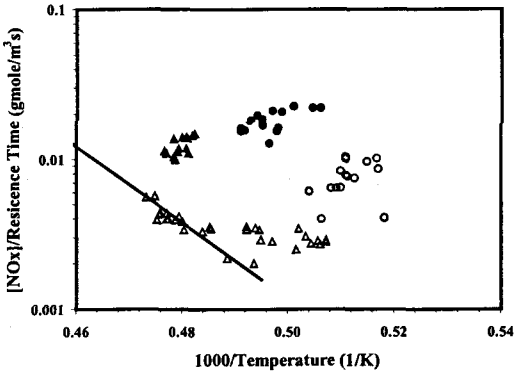

Figure 4. The radiant fraction data of Fig. 3(b) are plotted against the global residence time (Legend as for Fig. 2).

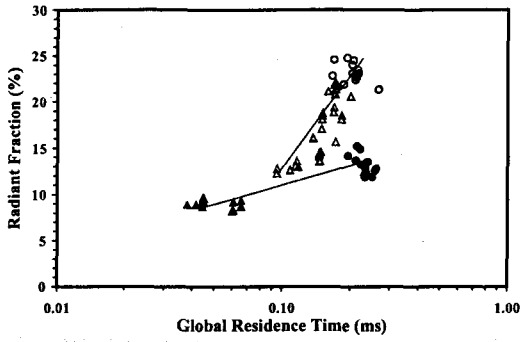

Figure 5. Time-temperature scaling (Legend as for Fig. 2).